JOURNAL OF Applied Polymer SCIENCE

Effect of coupling agent on structure and properties of micro-nano composite fibers based on PET

Zhaohui Jiang,[1] Pibo Ma,[2] Zengge Guo,[1] Zhao Jia,[1] Congcong Pu,[1] Changfa Xiao[3]

[1]Lutai School of Textile and Apparel, Shandong University of Technology, Zibo 255049, China
[2]Key Laboratory of Eco-Textiles, Ministry of Education, Jiangnan University, Wuxi 214122, China
[3]Key Laboratory of Fiber Modification and Functional Fiber, Tianjin Polytechnic University, Tianjin 300387, China
Correspondence to: P. B. Ma (E-mail: tjjzh_2005@163.com)

ABSTRACT: Poly(ethylene terephthalate) (PET)/carbon black (CB) micro–nano composite fibers were manufactured by melt spinning method. To achieve good dispersion, nano-CB particles were modified by coupling agent (CA). The effect of CA on structure and properties of the fibers were investigated via scanning electron microscopy (SEM), tensile testing, differential scanning calorimetry (DSC), wide-angle X-ray diffraction (WAXD), sonic orientation, and birefringence, respectively. At 2 wt % CA dosage, CB particles present the optimal dispersion in the fibers, shown in SEM images. Besides, the fibers possess the maximum breaking strength, the lowest crystallization temperature, and the highest crystallinity. After CA modification, the superior interfacial structure between PET and CB is beneficial to improve mechanical properties of the fibers. The well dispersed CB particles provide more heterogeneous nucleation points, resulting in the highest crystallinity. Furthermore, the fibers with 2 wt % CA dosage possess the maximum orientation and shrinkage ratio. According to Viogt–Kelvin model, the thermal shrinkage curves of the fibers can be well fitted using single exponential function. The three-phase structure model of crystal phase–amorphous phase–CB phase was established to interpret the relationship among shrinkage, orientation, and dispersion of CB particles. © 2016 Wiley Periodicals, Inc. J. Appl. Polym. Sci. **2016**, *133*, 43846.

KEYWORDS: fibers; properties and characterization; structure-property relations

Received 17 January 2016; accepted 25 April 2016
DOI: 10.1002/app.43846

INTRODUCTION

Poly(ethylene terephthalate) (PET) fiber has been extensively used in clothing, domestic, and industrial fields[1–4] owing to its good mechanical properties, chemical and thermal stability, wearability, processability, and low cost. However, the traditional dyeing process (post dyeing) for PET fiber is conducted under boiling and high-pressure conditions,[5–9] which goes against energy saving and emission reduction. Therefore, some attempts have been tried to develop easy dyeable PETs such as cationic dyeable polyester,[10,11] dyeable polyester with disperse dyes,[12–16] carrier dyeable polyester,[17–19] and acid dyeable polyester,[20] which are generally regarded as modified PET materials. Even so, some of the challenges including low dye uptake, non-uniform coloration, and uneasy to dye dark still remain. Fortunately, dope dyeing technique can largely alleviate these issues.

Dope dyeing is an "aged" technique. In the 1950s, PET fibers can only be dyed by dope dyeing due to the restriction of dyeing technology and dyestuffs. Besides, the difficulties lie in monotonous color and unable dyeing when they are blended with nature fiber like cotton. In the 1960s, disperse dyestuffs, high temperature and pressure techniques are applied to solve the post-dyeing problems of polyester fiber and fabric, making post dyeing move into high gear. Nowadays, centering on the issues that post-dyeing brings with, ranging from high energy consumption, water pollution to security of textiles, people have to develop more dyeing techniques to solve those problems. Furthermore, for dope dyeing technique, it is an important innovation in beautiful hues, whole color system, varied types, and standard color card production. Consequently, dope dyeing can be considered as a "young" technique, featuring energy saving, water saving, and environment friendly. Among other things, dope dyeing has been endowed with the new meaning that multi-function combination can be realized in the process, such as antiflaming, antistatic, antibacterium, etc. At present, most of the dope dyeing are conducted by masterbatch method. During the process, the masterbatch is added into bulk chips (polymer matrix), followed by further melt-blending. Moreover, inorganic nanoparticles are commonly employed as functional components in the masterbatch. It involves the dispersion of inorganic particles in polymer matrix. To achieve good dispersion, nanoparticles are often modified by physical or chemical methods, in which the modification by coupling agent (CA) is one of the most commonly used one. In the process of dope

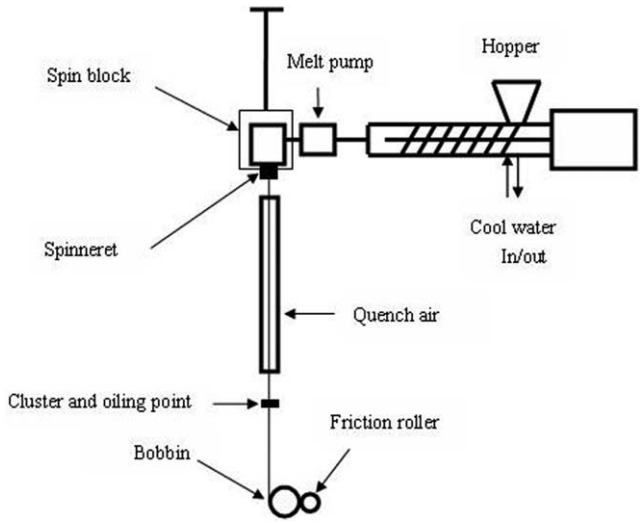

Figure 1. Schematic diagram of the spinning device.

dyeing, polypropylene (PP) products are usually dyed dark black using nano-carbon black (CB) particles. Meanwhile, CB particles play the role of good conductive media. For example, Jin *et al.*[21,22] investigated the effect of CB modified by CA (NDZ-101) on electrically conductive properties of masterbatch and PET fibers. The results indicate that CA can reduce the percolation threshold of the final fibers.

In this work, PET/CB micro–nano composites fibers were manufactured by melt spinning method. To achieve good dispersion, CA (NDZ-109) was selected as a modifier for CB particles.[23] The effect of CA on structure and properties of the fibers were also investigated. Furthermore, the structure model among crystalline phase, amorphous phase, and inorganic particle phase was established.

EXPERIMENTAL

Materials

PET, $\eta = 0.67$ dL/g, was commercially available and provided by Jiangsu Hengli Chemical Fiber Co., Ltd, Suzhou, Jiangsu Province, China. Carbon black (CABOT, MONARCH800), characterized in our previous study,[23] was obtained from Shanghai Oman Chemical Co., Ltd, Shanghai, China. Isopropyl alcohol, analytically pure, was provided by Beijing Chemical Plant, Beijing, China. The titanate coupling agents (NDZ-109) were purchased from Nanjing Shuguang Chemical Group Co., Ltd, Nanjing, Jiangsu Province, China. Its molecular structure is also shown in the literature.[23] Besides, the preparation of PET/CB/CA masterbatch is described therein.

Preparation of PET/CB Micro–Nano Composite Fibers

After pre-dried at 85 °C for 2 h, PET chips and PET/CB/CA masterbatch were dried in rotating drum vacuum oven at 150 °C for 5 h. A special twin screw extruder (Beijing Chonglee Machinery Engineering Co., Ltd, China), shown in Figure 1, was employed to carry out the experiment. Melt spinning was performed at the extrusion temperature of 285 °C with a spinneret plate having 48 holes (diameter 0.3 mm). The extruded fine streams were air-cooled, and they were formed into as-spun fibers at the speed of 3000 m/min. The spinning conditions of the fibers are summarized in Table I.

Scanning Electron Microscopy Observation

For scanning electron microscopy (SEM; ISM-6360, Japan) observation, the samples were attached to sample supports and sputter-coated with a gold layer. The observations of the outer surfaces and cross-sections were performed at an acceleration voltage of 12 kV.

Tensile Properties/Shrinkage

Tensile testing was performed on a universal testing machine (Model 2343, Instron, USA) according to GB/T 14344-2008 (Standard of the Peoples' Republic of China). The fibers were tested using a gauge length of 200 mm and a constant crosshead speed of 200 mm/min.

Shrinkage was calculated according to the percentage change in length when the fiber (100 mm) was exposed to hot air in a vacuum oven at 130 °C for at least 40 h.

Differential Scanning Calorimeter

A differential scanning calorimeter (DSC) thermal analyzer (Pyris 1, Perkin Elmer, USA) was used for DSC analysis. Each sample of 5–10 mg was weighed before being placed in DSC span. Under nitrogen atmosphere, it was heated from room temperature to 285 °C at a heating rate of 20 °C/min. The sample was kept for 5 min at 285 °C to eliminate thermal history. Then the melt was cooled to room temperature at a cooling rate of 20 °C/min. Crystallinity of the fibers (X_c) can be calculated according to the following equation[24–26]:

$$X_c = \frac{\Delta H_m - \Delta H_{cc}}{\Delta H_c^0 \times (1-\phi)} \times 100\% \quad (1)$$

where ΔH_{cc} is the cold crystallization enthalpy, ΔH_c^0 refers to enthalpy of 100% crystalline PET, considered as 135.8 J/g[27,28] and ϕ is weight ratio of the CB particles.

Wide-Angle X-ray Diffraction

Wide-angle X-ray diffraction (WAXD) measurements were performed in a diffractometer(X'Pert, PANalytical, the Netherlands) with Cu source ($\lambda = 1.54$ Å), scanning 2θ from 6° to 36°, at a step of 0.05°. The generator tension was 50 kV at 20 mA. After cut into small pieces, all the specimens were compression molded.

Table I. Spinning Conditions of the Fibers

Items	Conditions
Pre-crystallization temperature (°C)	85
Drying temperature (°C)	150
Barrel temperatures of the extruder (°C)	260/270/280/285/285/285
Spinning speed (m/min)	3000
Mass flow rate (g/min)	42
Pressure after melt filter (MPa)	7
Spinning pack pressure (MPa)	11
Temperature of heat medium (°C)	290
Side blowing temperature (°C)	20
Side blowing speed (m/s)	0.6
Moisture of Side blowing air (%)	70%-80%
Spinneret size (pores)	48

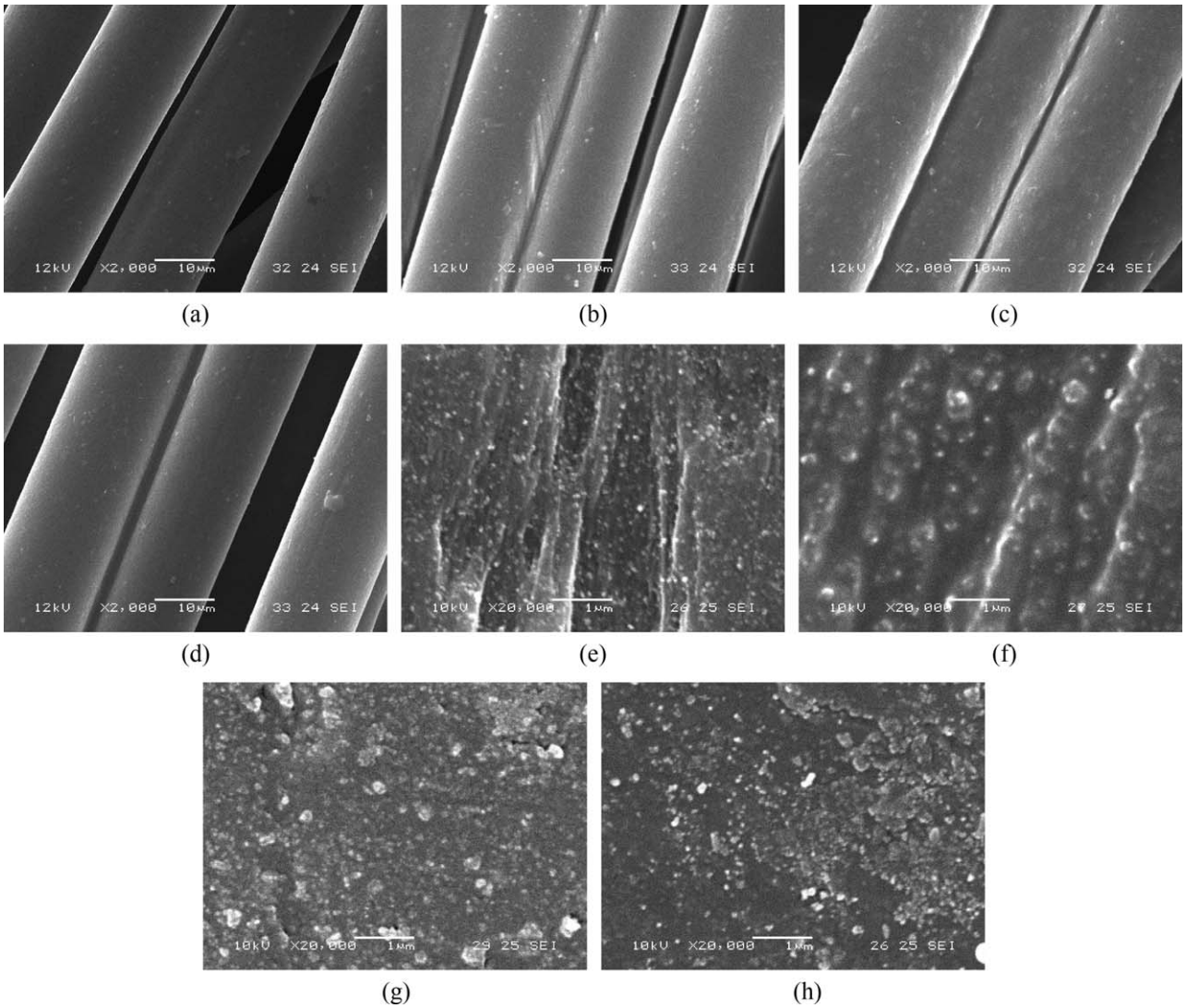

Figure 2. SEM images of the fibers with different CA dosages: (a–d) surface; (e–h) cross section; (a,e) 2 wt %; (b,f) 4 wt %; (c,g) 6 wt %; (d,h) 8 wt %.

Birefringence

Birefringence (Δn) was measured with a polarizing microscope equipped with a Berek compensator. The diameter of the fiber was measured with the aid of an eyepiece micrometer. An average of five different measurements was reported.

Sonic Orientation Factor

The sound velocity values of the fibers were obtained with the aid of sound velocimeter (SSY-1, institute of Applied Chemistry, Chinese Academy of Sciences). The sonic orientation factor of the fibers can be determined by the following equation:

$$f_s = 1 - \frac{C_u^2}{C^2} \tag{2}$$

where C_u is the sound velocity of random orientation samples and C is sound velocity of the fibers.

RESULTS AND DISCUSSION

Effect of CA on Dispersion of the CB Particles

Figure 2 illustrates the SEM images of the micro–nano fibers with different CA dosages (CA weight accounts for CB weight). Seen from Figure 2, when the dosage of CA is 2 wt %, CB particles are dispered uniformly and their diameters are smaller. As shown in Figure 2(a,e), the compatibility between CB particles modified by CA and PET matrix is improved at an appropriate amount of CA dosage, thus favoring the dispersion of CB particles. Moreover, the reaction mechanism among PET, CB, and CA are illustrated in our previous article.[23] However, with the increase of CA dosages, larger CB aggregates appear as shown in Figure 2(f–h). These results from the fact that the excessive CA anchoring on the surfaces of CB particles forms numerous physical entanglement points. Thus, the CA molecular chains on the surface of adjacent CB particles tend to intertwist together, causing the aggregation of CB particles.

Effect of CA on Tensile Properties of the Fibers

The tensile properties of the as-spun fibers are listed in Table II. As shown in Table II, the fibers with CA dosage of 2 wt % present the maximum breaking strength and the minimum elongation at break, and their CV values are the least ones. The CA molecules with functional groups can simultaneously react with PET and CB. This builds "molecular bridges" between PET and

Table II. Mechanical Properties of the As-Spun Fibers with Different CA Dosages

CA dosages (wt %)	Tenacity (cN/dtex)	Tenacity CV (%)	Elongation (%)	Elongation CV (%)	Modulus (cN/dtex)
2	2.1	5.5	130.0	2.6	26.3
4	2.0	6.7	138.2	3.0	25.3
6	1.9	4.1	136.3	3.2	24.4
8	1.8	9.1	140.8	6.9	24.3

CB, forming good interfacial structure. However, there is an optimal value for CA dosages. At this point, CB particles are dispersed uniformly in the fiber. When the fibers are subjected to tensile stress, these CB particles play a role of making stress distribution uniform, which is beneficial to improve mechanical properties of the fibers. When CA dosage is too small, there are no enough CA molecules grafted onto the surfaces of CB particles, causing the agglomeration of CB particles. When CA dosage is excessive, a multi molecular physics adsorption layer is formed by the lipophilic ends of the excess CA molecules. The multi molecular adsorption layer is easy to form physical entanglement points due to their good compatibility. As a result, the CB particles tend to reunite into larger agglomerates due to mutual entanglement, forming interfacial defects. This is also not conducive to improve mechanical properties of the fibers.

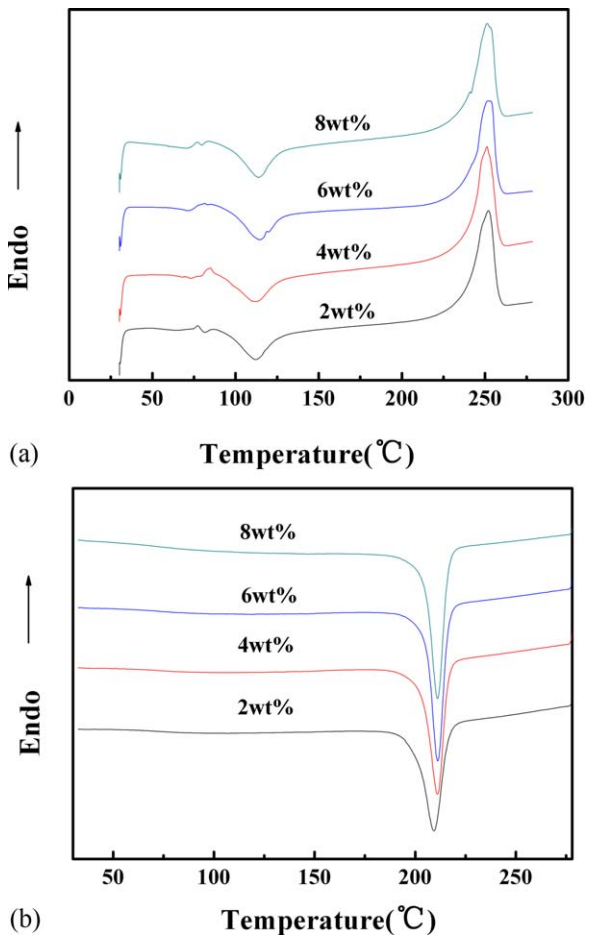

Figure 3. DSC curves of the fibers with different CA dosages: (a) heating, (b) cooling. [Color figure can be viewed in the online issue, which is available at wileyonlinelibrary.com.]

Effect of CA on Melting and Crystallization Properties of the Fibers

Figure 3 shows the DSC curves in the courses of heating and cooling, and the thermal transition parameters from the curves are listed in Table III. As shown in Table III, the glass transition temperature (T_g) of the fibers is lowest at CA dosage of 2 wt %, which indicates the best compatibility between PET and CB.[29,30] Besides, the fibers with CA dosage of 2 wt % possess the lowest crystallization temperature. The CB surfaces are grafted with a layer of CA molecules, which forms numerous physical and chemical crosslinking points with molecular chains of PET. This delays the heterogeneous nucleation effect of CB particles, decreasing the crystallization temperature. It stems from the interaction between PET and CB, which restricts the movement of chain segments and hinders the folding of PET molecular chains into lamella, inhibiting the crystallization of PET. However, the fibers with 2 wt % CA dosage show the maximum crystallinity, indicating that it realizes the best dispersion of CB particles. This provides more nucleating points for PET crystallization. In DSC curves during heating process, the fibers with 2 wt % CA dosage are provided with the lowest cold crystallization temperature and the highest melting temperature. It is because that the contribution of crystallization mainly comes from the formation of crystal nucleus during the process of cold crystallization. The well dispersed CB particles can provide numerous nuclei. This also indirectly states that the fibers with 2 wt % CA dosage possess the most uniform dispersion of CB particles.

Figure 4 illustrates WAXD spectra of the fibers with different CA dosages. The characteristic diffraction peaks of (010), (110), and (100) crystal plane for PET are overlapped, leaving the

Table III. Thermal Transition Parameters of the Fibers with Different CA Dosages

CA dosages (wt %)	2	4	6	8
T_g (°C)	74.6	81.7	76.4	75.3
T_{cc} (°C)	111.9	111.9	114.6	113.9
T_m (°C)	252.0	251.3	251.6	251.3
ΔH_m (J/g)	47.2	47.3	44.9	46.6
ΔH_{cc} (J/g)	23.3	28.7	25.2	26.6
X_c (%)	22.0	17.1	18.1	18.4
T_{mc} (°C)	209.5	211.1	211.1	211.1

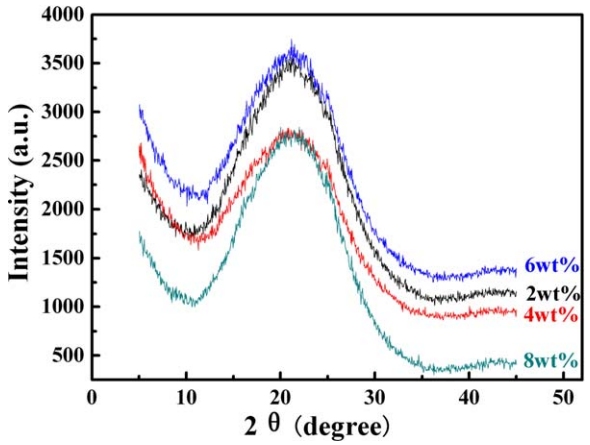

Figure 4. WAXD patterns of the fibers with different CA dosages. [Color figure can be viewed in the online issue, which is available at wileyonlinelibrary.com.]

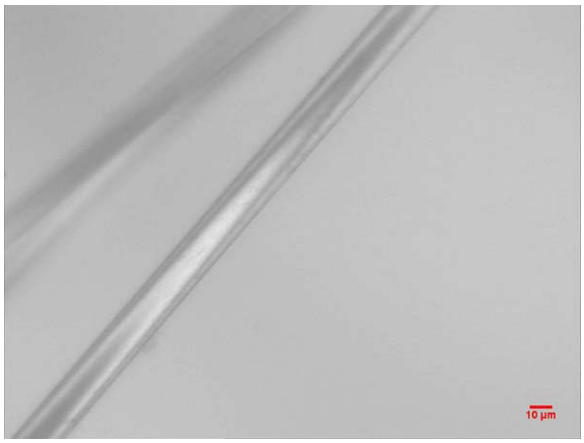

Figure 5. Polarizing microscope images of the fibers (400×). [Color figure can be viewed in the online issue, which is available at wileyonlinelibrary.com.]

dispersive "steamed bread" peaks with amorphous structure characteristics. By comparison of the peak sharpness, it comes to the conclusion that the fibers with 2 wt % CA dosage present the maximum degree of crystallization, which is consistent with DSC results.

Effect of CA on Orientation Properties of the Fibers

Because of the imperfection of crystalline structure of the as-spun fibers, diffraction peaks of the typical crystal planes in the WAXD spectra do not appear, and the orientation function of the crystalline region cannot be obtained. Accordingly, we cannot distinguish the orientation of crystalline region and amorphous region. The method of sound velocity is suitable to characterize overall orientation of the fibers. Prior to calculating the sonic orientation factor, it is necessary to obtain the sound velocity values of PET/CB fibers with completely random orientation. Considered non-oil fibers as random orientation samples, the measured sound velocity of the samples is 1.47 km/s, which is consistent with the reported value in the literature.[31] The orientation parameters of the as-spun fibers with different CA dosages are listed in Table IV. Although the samples are as-spun fibers spun at 3000 m/min, the anisotropy of the fibers is clearly visible (shown in Figure 5). The birefringence and sonic orientation factor both show that the orientation of the fibers with 2 wt % CA dosages is slightly greater than those of other fibers.

Table IV. Orientation Parameters of the As-Spun Fibers with Different CA Dosages

CA dosages (wt %)	Birefringence	Sound velocity (km/s)	Sonic orientation factor (f_s)
2	0.038	1.69	0.31
4	0.037	1.67	0.30
6	0.035	1.64	0.27
8	0.037	1.67	0.30

Relationship among Shrinkage, Orientation, and Dispersion

The orientations of the fiber with different CA dosages are close to each other, so it is difficult to accurately compare orientation of the fibers. For as-spun fibers, the crystallinity and crystal orientation are very small. Accordingly, the orientation is mainly contributed by the orientation of amorphous region. Moreover, the essence of thermal shrinkage is the disorientation of amorphous region of fibers. Therefore, the shrinkage of fibers in hot air can be employed to evaluate the orientation of amorphous region. The relationship curves of the fibers between the residual relative length $[1-s(t)]$ and the shrinkage time (t) in hot air (87 °C) are illustrated in Figure 6. According to Viogt–Kelvin model, the dynamic equation of the isothermal shrinkage is as follows:

$$1-s(t)=A_1 e^{-t/\tau_1}+A_2\cdot e^{-t/\tau_2}+\cdots+1-s_0 \quad (3)$$

where $s(t)$ represents shrinkage ratio at time t, A_1 and A_2 are contributions of the corresponding viscoelastic units to shrinkage ratio, τ_1 and τ_2 are specific relaxation times of the corresponding viscoelastic units, and s_0 is the shrinkage ratio of fibers when t tends to infinity.

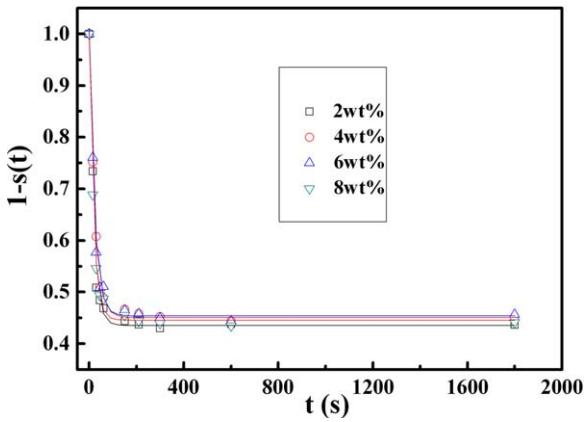

Figure 6. Relationship between $1-s(t)$ and t of the fibers. [Color figure can be viewed in the online issue, which is available at wileyonlinelibrary.com.]

Table V. Fitting Parameters from Heat Shrinkage Curves of the Fibers

CA dosages (wt %)	$1 - s_0$ ($\times 10^2$)	A ($\times 10^2$)	τ (sec)	R^2 ($\times 10^2$)
2	43.6	57.3	18.9	98.8
4	45.1	55.3	23.0	99.7
6	45.4	55.2	22.2	99.3
8	44.6	55.3	18.3	99.7

The variation trend of residual relative length is accurately fitted using single exponential function. The fitting parameters are shown in Table V. When CA dosage is 2 wt %, the specific relaxation time of the fibers is the minimum, while the shrinkage ratio of the fibers is the maximum. It can be concluded that the fibers with 2 wt % CA dosage have the maximum orientation. This is in accord with the results from birefringence and sound velocity method.

Based on the two-phase structure model of crystal phase–amorphous phase, the three-phase structure model of crystal phase–amorphous phase–CB phase was established to interpret the relationship between the orientation of amorphous region and CB dispersion. Because the crystalline region is relatively stable, the majority of CB particles are distributed in amorphous region. The schematic diagram of amorphous structure of the fibers is illustrated in Figure 7. There is a strong interaction between CA molecules anchored on surfaces of CB particles and PET macromolecular chains. This forms an adsorption orientation effect on PET chains, resulting in extension of the chains and increasement of the orientation. In the case of good CB dispersion, more PET macromolecular chains are adsorbed onto the surfaces of CB particles and they extend fully. While CB particles are poorly dispersed, the total surface area of CB particles decreases, weakening the adsorption orientation effect. Combined with SEM results, when CA dosage is 2 wt %, the CB particles are well dispersed and uniformly distributed, so the orientation of the fibers with 2 wt % CA dosage is relatively high, which is consistent with the result of thermal shrinkage.

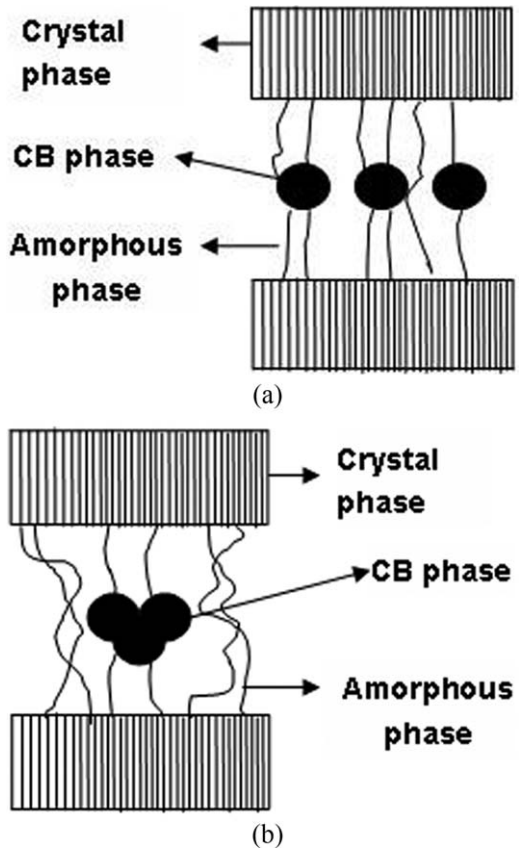

Figure 7. Schematic diagram of amorphous structure for fibers with different dispersion states (a) good dispersion, (b) poor dispersion.

CONCLUSIONS

PET/CB micro–nano composite fibers were manufactured by melt spinning method. Prior to spinning, PET/CB masterbatches, in which CB particles were modified by CA, were prepared using separate feeding technique. Then, masterbatch-dilution technique was employed to fabricate micro–nano composite fibers. SEM results show that the fibers present a good dispersion of CB particles when the dosage of CA is 2 wt %. Meanwhile, at the CA dosage of 2 wt %, the fibers provide with the optimal tenacity due to the good interfacial structure between PET and CB. DSC curves demonstrate that the fibers with 2 wt % CA dosage present the lowest crystallization temperature. This is attributed to the inhibiting crystallization effect of CA molecules. However, the fibers with 2 wt % CA dosage possess the greatest crystallinity, confirmed by DSC and WAXD. This indirectly indicates that CB particles achieved optimal dispersion and they provide more heterogeneous nucleation points during the process of PET crystallization. Moreover, CA also plays a significant role on orientation of the fibers. The orientation of fibers with 2 wt % CA dosages is slightly greater, which is demonstrated by birefringence and sound velocity. According to Viogt–Kelvin model, the thermal shrinkage curves of the fibers were fitted using single exponential function. The fitting parameters suggest that for the fibers with 2 wt % CA dosage, the specific relaxation time is the minimum and the shrinkage ratio is the maximum. Ascribed the essence of hot shrinkage to disorientation of amorphous region, the conclusion that the fibers with 2 wt % CA dosages have the maximum orientation. Furthermore, the relationship among shrinkage, orientation and dispersion of CB particles was revealed, and the three-phase structure model of crystal phase–amorphous phase–CB phase was established to interpret the relationship.

ACKNOWLEDGMENTS

The authors gratefully acknowledge the financial support of doctoral scientific research funds of Shandong University of Technology (4041-413047), the open project program of Key Laboratory of Eco-Textiles, Ministry of Education, Jiangnan University (No. KLET1401), Shandong Province Higher Educational Science and Technology Program (J14LA56), and Shandong Provincial Natural Science Foundation, China (ZR2014EMP004).

REFERENCES

1. Wang, S. H.; Hou, W. S.; Wei, L. Q.; Dai, J. M.; Jia, H. S.; Liu, X. G.; Xu, B. S. *J. Appl. Polym. Sci.* **2009**, *112*, 1927.

2. Karaca, E.; Ozcelik, F. *J. Appl. Polym. Sci.* **2007**, *103*, 2615.
3. Jeon, Y. P.; Cox, L. C. *J. Appl. Polym. Sci.* **2008**, *110*, 2153.
4. Chidambaram, D.; Venkatraj, R.; Manisankar, P. *J. Appl. Polym. Sci.* **2003**, *87*, 1500.
5. Saus, W.; Knittel, D.; Schollmeyer, E. *Text. Res. J.* **1993**, *63*, 135.
6. Hou, A. Q.; Chen, B.; Dai, J. J.; Zhang, K. *J. Clean. Prod.* **2010**, *18*, 1009.
7. Bendak, A.; Raslan, W. M. *J. Appl. Polym. Sci.* **2008**, *108*, 7.
8. Bang, H. J.; Kim, H. Y.; Jin, F. L.; Park, S. J. *J. Ind. Eng. Chem.* **2011**, *17*, 805.
9. Clerck, K. D.; Oostveldt, P. V.; Rahier, H.; Mele, B. V.; Westbroek, P.; Kiekens, P. *Polymer* **2004**, *45*, 4105.
10. Lee, M. S.; Lee, M.; Wakida, T.; Saito, M.; Yamashiro, T.; Nishi, K.; Inoue, G.; Ishida, S. *J. Appl. Polym. Sci.* **2007**, *104*, 2423.
11. Ren, Z. P.; Qin, C. X.; Tang, R. C.; Chen, G. Q. *Color Technol.* **2012**, *128*, 147.
12. Ujhelyiova, A.; Bolhova, E.; Oravkinova, J.; Tiňo, R.; Marcinčin, A. *Dyes Pigm.* **2007**, *72*, 212.
13. Giorgi, M. D.; Cadoni, E.; Maricca, D.; Piras, A. *Dyes Pigm.* **2000**, *45*, 75.
14. Kim, T. K.; Son, Y. A.; Lim, Y. J. *Dyes Pigm.* **2005**, *67*, 229.
15. Sadeghi-Kiakhani, M.; Gharanjig, K. *J. Surfact. Deterg.* **2015**, *18*, 47.
16. Georgiadou, K. L.; Tsatsaroni, E. G.; Eleftheriadis, I. C.; Kehayoglou, A. H. *J. Appl. Polym. Sci.* **2002**, *83*, 2785.
17. Ghaharpour, M.; Rashidi, A.; Tayebi, H. *World Appl. Sci. J.* **2011**, *14*, 1291.
18. Karanikas, V.; Nikolaidis, N.; Tsatsaroni, E. *Text. Res. J.* **2013**, *83*, 450.
19. Seok, B. J.; Jong, H. P.; Joonseok, K.; Sung, D. K. *Fiber Polym.* **2006**, *7*, 174.
20. Wu, J.; Chu, C. C. *Acta Biomater.* **2012**, *12*, 4314.
21. Jin, X.; Xiao, C. F.; An, S. L.; Jia, G. X. *J. Appl. Polym. Sci.* **2006**, *102*, 4144.
22. Jin, X.; Xiao, C. F.; An, S. L.; Jia, G. X.; Wang, Y. Y. *Int. Polym. Proc.* **2006**, *21*, 348.
23. Jiang, Z. H.; Jin, J.; Xiao, C. F.; Li, X. *Colloid Surf. A: Physicochem. Eng. Asp.* **2012**, *395*, 105.
24. Jiang, Z. H.; Xiao, C. F.; Wang, X.; Hu, X. Y. *Chin. J. Polym. Sci.* **2010**, *28*, 721.
25. Kong, Y.; Hay, J. N. *Polymer* **2002**, *43*, 3873.
26. Li, Z. F.; Luo, G. H.; Wei, F.; Huang, Y. *Compos. Sci. Technol.* **2006**, *66*, 1022.
27. Bendak, A.; Kantouch, A.; Nasr, M. F. *J. Appl. Polym. Sci.* **1997**, *65*, 2773.
28. Ahani, M.; Khatibzadeh, M.; Mohseni, M. *J. Ind. Eng. Chem.* **2013**, *19*, 1956.
29. Rõo, C. D.; Ojeda, M. C.; Acosta, J. L. *Eur. Polym. J.* **2000**, *36*, 1687.
30. Herrero, C. R.; Morales, E.; Acosta, J. L. *J. Appl. Polym. Sci.* **1994**, *51*, 1189.
31. Huang, X. G.; Zhang, W. Z. *Synth. Fiber* **1981**, *4*, 24.